Kulowski *Heritage Science* (2022) 10:104
https://doi.org/10.1186/s40494-022-00713-6

Heritage Science

RESEARCH ARTICLE Open Access

Do Leonardo da Vinci's drawings, room acoustics and radio astronomy have anything in common?

Andrzej Kulowski*

Abstract

After introducing Leonardo da Vinci's (LdV) predecessors in the field of light propagation research, his drawings on the topic of reflecting light by a spherical mirror are analysed. The discovery of LdV is presented, according to which, at an infinitely distant source of rays, a small fragment of the canopy is enough to generate a focus, while the rest of the mirror forms a caustic for which LdV did not indicate an application. An analytical description of the energy concentration in the focus and on the caustic is given, together with its reference to the geometric representation of the acoustic field in rooms. Based on the general principles of wave motion, symmetry is shown in the description of energy relations in acoustics and electromagnetism. It is explained why in the sound field in existing halls, instead of a whole caustic only its cusp is observed, which is perceived as a point-like sound focus. The size of the mirror aperture, shown graphically by LdV, is determined. How the development of receiving techniques increased the mirror aperture compared to the LdV estimate is also shown. The implementation of these improvements is presented via the example of the Arecibo and FAST radio telescopes.

Keywords: Leonardo da Vinci, Caustic, Spherical reflector, Room acoustics, Arecibo, FAST

Introduction

Early considerations about the propagation of light lie at the beginning of the research discipline that has developed into today's physics. One of the earliest accounts on optics, i.e. the use of instruments interfering with the course of light, is the story from ancient times about Archimedes setting fire to Roman ships besieging Syracuse with the use of mirrors reflecting sunlight [1]. A later treatise by Ptolemy from the second century AD is another significant work of the antiquity period concerning the study of optics [2]. The scientific considerations he initiated were continued in the Middle Ages in the Islamic world. Leonardo da Vinci (LdV) carried out his works in reference to this tradition [3]. He paid particular attention to the application of the rules of geometric optics in architecture, painting and graphics, including studies in the field of perspective and chiaroscuro.

Leonardo's sketches on optics include studies of a particular form of focusing rays of light, nowadays known as caustics (Fig. 1). In the convention of geometric optics, caustic is a surface formed by rays tangent to it after reflection from a concave surface or as a result of propagation in an inhomogeneous medium. Under certain circumstances, a cusp may form on the caustics. In the mathematical description of caustics, it corresponds to a singularity, i.e. the parameters of the field of rays at this point tend to infinity. The physical counterpart of the caustic cusp is the focus of the mirror. The focus can also form without a caustic accompanying it, but it only applies to a few specific cases, among them a source in the centre of a spherical reflector, a parabolic reflector with an infinitely distant source on its geometric axis, or an ellipsoidal reflector with a source in one of its foci.

*Correspondence: kulowski@pg.edu.pl

Faculty of Architecture, Gdańsk University of Technology, ul. Gabriela Narutowicza 11/12, 80-233 Gdańsk, Poland

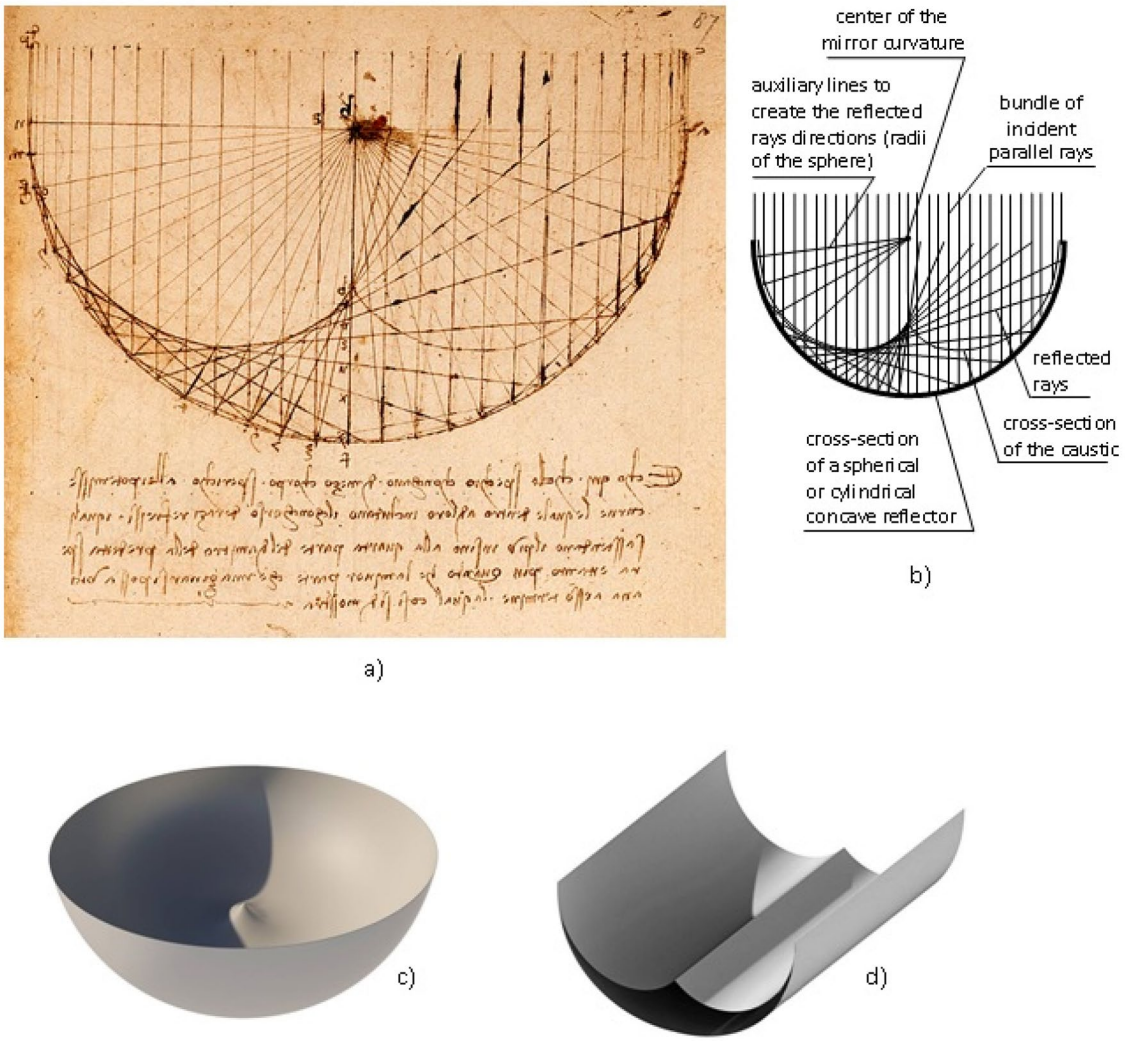

Fig. 1 **a** Drawing of caustic from Leonardo da Vinci's notebook. The note below the picture in Fig. 1a, made in Leonardo's famous reverse script, says that in concave mirrors of equal diameter, the one that has the shallower curve will concentrate the largest number of reflected rays onto a focal point, and "as a consequence, it will kindle a fire with greater rapidity and force" [9] © British Library Board, Source: Arundel MS 263. **b** Details of Leonardo's drawing, (**c**, **d**) 3D views of the caustics created by spherical and cylindrical concave mirrors [10]

Leonardo showed that with an infinitely distant light source, only a small part of the spherical mirror is involved in creating the focus. The remainder of the mirror only forms caustics and is useless for focal formation, leading to important practical conclusions. The idea of focusing light in this way is attributed to Archimedes, who lived many centuries earlier, but the quantitative analysis shown graphically in Fig. 2 is Leonardo's personal contribution to the study of the principle of the operation of a concave mirror.

Against this historical background, the article discusses the formation of foci and caustics in the acoustic field and in the electromagnetic field. Observations of room acoustics indicate that in the audible frequency range, caustics are so blurred by diffuse sound, wave reflections and interference that it is reduced to its singularity. The observed form of caustic is then a compact area of increased sound pressure with a size dependent on the wavelength, which is the result of a diffractive broadening of a point-like focus known from graphic analysis. This occurs when the wavelength is of the same order or slightly shorter than that of the objects in the acoustic field, which is typical for rooms.

When the wavelength is much shorter than the objects in the wave field, the blur effect is much smaller and the caustic act as a clearly identified energy focus area.

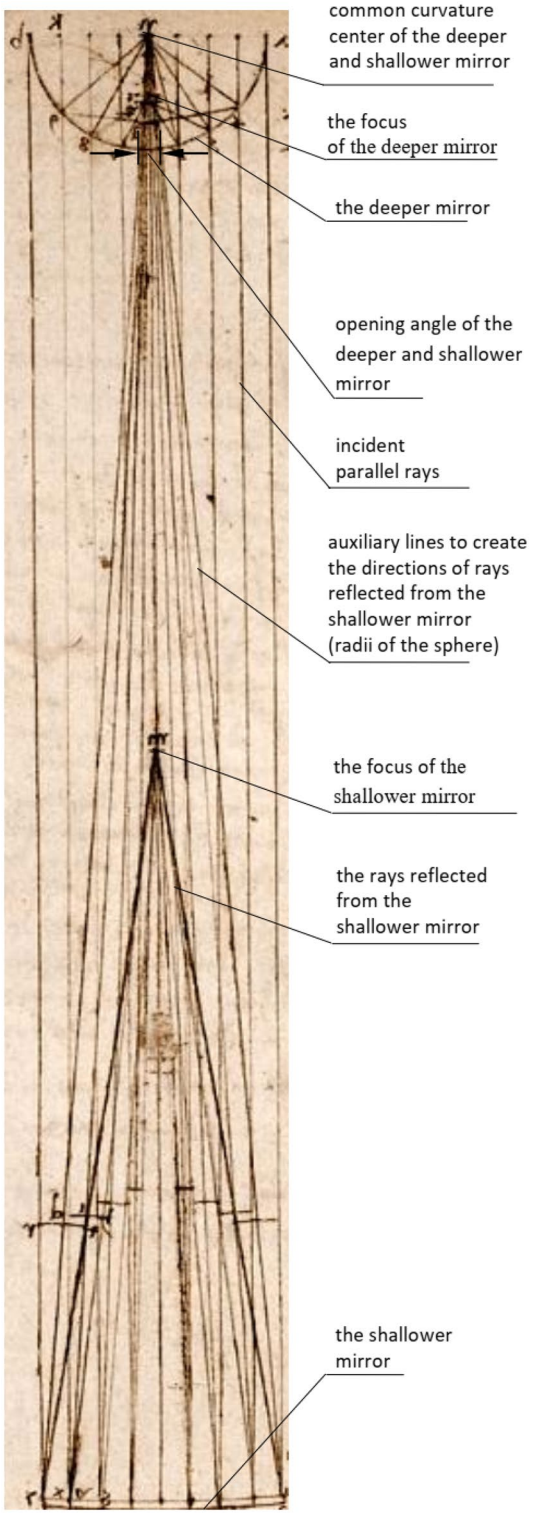

Fig. 2 Illustration of Leonardo's concept, in which a shallower mirror (bottom) concentrates a larger number of rays than the mirror with a deeper bowl of the same diameter (top) [9]. © British Library Board, Source: Arundel MS 263

Caustics formed in this way are present in many fields of technology and science concerning the propagation of light, ultrasounds and electromagnetic waves, e.g. hydroacoustics, aeroacoustics, laser technology, and even radio astronomy [4–6].

Based on the inspiration of caustic drawings in LdV's works and his considerations on reflecting light by a concave mirror, the article presents a mathematical description of the effect of focusing rays. Against this background, the phenomena occurring on caustics in acoustic and electromagnetic fields are presented, taking into account their wave nature.

The main goal of this paper is to investigate the extent to which LdV observations of the formation of caustics and foci are present in modern technology. The article shows how LdV's estimate of a mirror aperture has expanded as radio waves receiving techniques have developed. The presence of Leonard's thoughts in these activities is demonstrated through the example of the large radio telescopes in Arecibo (Puerto Rico) and Dawodang (China).

Caustics in the legacy of Leonardo da Vinci

The drawings of caustics in Leonardo da Vinci's notes refer to his research in the field of optics in the years 1510–1515 [7, 8]. You can find in them many sketches of caustics at different stages of their formation, the most complete drawing of a caustic is shown in Fig. 1. Leonardo made his drawing 500 years ago with such competence that in the article it is quoted as a perfectly valid example of applying the principles of geometric optics in the formation of caustics.

Leonardo was interested in the potential utility of concave mirrors as sources of heat, and the purpose of his research was to assess the focusing properties of a spherical mirror. Figure 2 shows the two mirrors differing in the depth of the canopy referred to in his reverse script in Fig. 1a. In his later works, Leonardo also planned to use the effect of focusing sunlight to heat or even boil water [11].

In light of today's level of knowledge, Leonardo's concept is obvious. However, he lived 500 years ago and the accuracy of his explanations must be considered admirable. The further part of the article shows that even in areas as distant from optics as room acoustics and radio astronomy, Leonardo da Vinci's concept can be found.

According to modern technical terminology, the fraction of the total energy incident on the mirror that is available at the receiver is called the mirror aperture. For the purposes of this article, the ratio of this area to the area of a full hemispherical mirror was adopted as the relative measure of aperture. Assuming the propagation

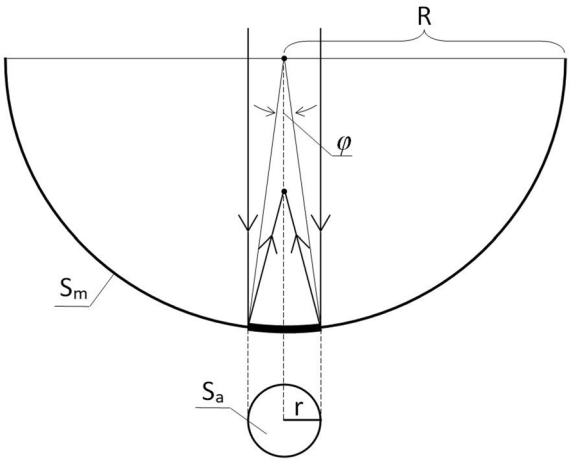

Fig. 3 Aperture of the shallower mirror from Fig. 2. S_m, *R* area and radius of the full hemispherical mirror, S_a, *r* area and radius of the aperture, *φ* opening angle read from Fig. 2, $\varphi = 10^{o}$

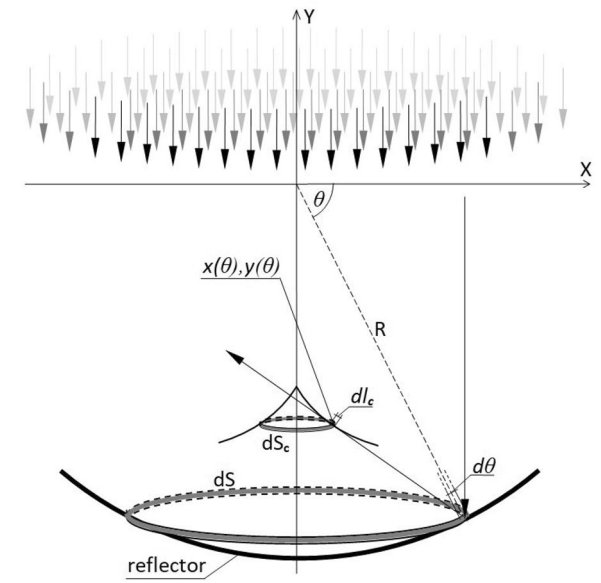

Fig. 4 Caustic formed by rays incident on a hemispherical reflector. *R* radius of the reflector, dS, dS_c ring on the reflector and on the caustic, *x(θ),y(θ)* Cartesian coordinates of the caustic (Eq. (3)), dl_c: the element of the section of the caustic [13]

and reflection of the rays are lossless, the relative aperture of the lower mirror shown in Fig. 2 is approximately 0.4% (Eqs. 1, 2).

For the opening angle $\phi = 10°$ (Fig. 3), the arc length r is

$$\mathrm{r} = \frac{\varphi/2}{180}\Pi\mathrm{R} = \frac{\Pi\mathrm{R}}{36} \tag{1}$$

and the aperture in relation to the surface of the full hemispherical mirror is

$$\frac{\mathrm{S_a}}{\mathrm{S_m}} = \frac{\Pi \mathrm{r}^2}{2\Pi\mathrm{R}^2} = \frac{1}{2}\left(\frac{\Pi}{36}\right)^2 = 0.0038 \cong 0.4\% \tag{2}$$

Analytic description of energy concentration on the caustic

The LdV sketches present the effect of the energy concentration on a caustic in a graphical form. This section gives a quantitative assessment of this effect in an analytical form, using the original LdV drawing.

Consider the rays coming from an infinitely distant source and falling on a hemispherical mirror as a collimated beam (Fig. 1a). After the reflection, the rays form the caustic described by Eq. (3) [12].

$$\begin{cases} \mathrm{x}(\theta) = \mathrm{R}\cos^3(\theta) \\ y(\theta) = \dfrac{\mathrm{R}}{2}\left(2\sin^3(\theta) - 3\sin(\theta)\right) \end{cases} \quad 0 \le \theta \le \Pi \tag{3}$$

To calculate the density of rays on a caustic, consider two rings inside the reflector's bowl: dS on its surface and dS_c on a caustic (Fig. 4) [12, 13]. Since all rays reflected from dS are tangent to dS_c, the relative density of rays on dS_c is dS/dS_c, where dS and dS_c are the surfaces of the rings.

The circumference and the width of the ring dS are $2\Pi\mathrm{R}\cos(\theta)$ and $\mathrm{R}\sin(\theta)\mathrm{d}\theta$, so

$$dS = 2\Pi\,\mathrm{R}^2\,\cos(\theta)\,\sin(\theta)\,d\theta \tag{4}$$

Likewise, the circumference and the width of the ring dS_c are $2\Pi x(\theta)$ and dl_c, so

$$dS_c = 2\Pi\, x(\theta)\, dl_c \tag{5}$$

where dl_c is the element of a section of a caustic

$$dl_c = \sqrt{\left(\frac{dx(\theta)}{d(\theta)}\right)^2 + \left(\frac{dy(\theta)}{d(\theta)}\right)^2}\, d\theta \tag{6}$$

and the derivatives over θ of *x(θ), y(θ)* are

$$\begin{cases} \dfrac{dx}{d\theta} = -3\mathrm{R}\cos^2(\theta)\sin(\theta) \\ \dfrac{dy}{d\theta} = -3\mathrm{R}\sin^2(\theta)\cos(\theta) - \dfrac{3}{2}\mathrm{R}\cos(\theta) \end{cases} \tag{7}$$

An elementary transformation gives

$$\sqrt{\left(\frac{dx(\theta)}{d(\theta)}\right)^2 + \left(\frac{dy(\theta)}{d(\theta)}\right)^2} = \frac{3}{2}R\cos(\theta) \tag{8}$$

Substitution of Eq. (7) to Eq. (6) yields

$$dl_c = \frac{3}{2}\mathrm{R}\cos(\theta)d\theta \tag{9}$$

so

$$dS_c = 3\Pi\mathrm{R}^2\ \cos^4(\theta)\, d\theta \tag{10}$$

Finally, if the rays incident on the mirror are distributed evenly on the y = 0 plane (Fig. 4), the relative density of rays C (θ) over the caustic is

$$C(\theta) = \frac{dS}{dS_c} = \frac{2\sin(\theta)}{3|\cos^3(\theta)|} \tag{11}$$

As θ tends to 0.5Π, C (θ) tends to infinity, which corresponds to the cusp formation on the caustic (Fig. 4). This singularity results from the caustic cross-sectional area dS_c tending to zero.

Let us denote the surface density of rays incident on the reflector as I_o [W/m^2]. The density of rays $C(\theta)$ in Eq. (11) multiplied by I_o can be interpreted as the surface density of energy over the caustic per unit of time, i.e. the intensity of the rays [W/m^2].

Equation (11) shows the surface power density on the surface of the caustic. It is a finite value except for the caustic cusp where C (θ) goes to infinity. However, when the energy density is considered on a cross sectiona plane of a caustic, a different result is obtained. For example, following the dashed line from point M towards the origin of the XY coordinate system (Fig. 6), the surface power density increases and reaches infinity at the caustic. In this case, the singularity applies to the entire caustic [6]. However, the article adopts the analysis of the surface power density not on a cross section of the caustic but on its surface.

When the absorption coefficient α of the reflector is taken into account, where α = 0 and α = 1 relate to a total reflection and total absorption, respectively, the rays relative intensity is

$$I_c(\theta) = \mathrm{I_o}(1-\alpha)\, C(\theta) = \mathrm{I_o}(1-\alpha)\frac{2\sin(\theta)}{3|\cos^3(\theta)|} \quad [\mathrm{W/m^2}] \tag{12}$$

The total intensity of the rays over the caustic $I_{c,res}(\theta)$ consists of the energy of incident rays I_o and the energy of the reflected rays on the caustic.

$$\begin{aligned} I_{c,res}(\theta) &= \mathrm{I_o} + \mathrm{I_o}(1-\alpha)\frac{2\sin(\theta)}{3|\cos^3(\theta)|} \\ &= \mathrm{I_o}\left(1 + (1-\alpha)\frac{2\sin(\theta)}{3|\cos^3(\theta)|}\right) \end{aligned} \tag{13}$$

The intensity level of the rays on the caustic, with I_o as the reference intensity, is then $L_{c,res}(\theta)$ (Fig. 5).

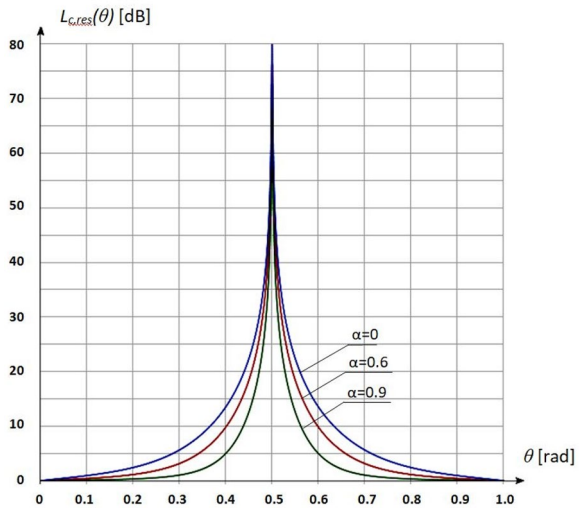

Fig. 5 Rays' intensity level $L_{c,res}(\theta)$ [dB] on the caustic. *α* absorption coefficient of the reflector [12]

$$\begin{aligned} L_{c,res}(\theta) &= 10\log\frac{I_{c,res}(\theta)}{\mathrm{I_0}} \\ &= 10\log\left(1 + (1-\alpha)\frac{2\sin(\theta)}{3|\cos^3(\theta)|}\right)[\mathrm{dB}] \end{aligned} \tag{14}$$

Caustics in the wave field

LdV's concept of caustics and its development, as shown in Fig. 2 and "Analytic description of energy concentration on the caustic", are based on the geometrical approach. Despite the roots that are distant in time, this approach is a fully functional model of energy propagation, currently used, for example, in room acoustics, optics and radio communication. This section describes the formation of caustics in a wave field, the manifestation of which is the interference of the incident wave with the wave reflected from the mirror.

Let us consider a plane wave of the wavelength λ much smaller than the diameter of the reflector D, incident on the reflector [12]. At the point in time t = 0, the wave front lies in the plane y = 0 (Fig. 6). Propagating deep into the reflector, the wave interferes with the reflected wave, creating an array of interference fringes filling the mirror's canopy and the space in front of it. The wave nature of the field is also the cause of wave deflection at the mirror edge [12]. The article concerns the caustic as presented by the LdV, therefore this chapter is limited to the description of the effect that occurs only in the caustic itself, i.e. the incident and reflected wave interference.

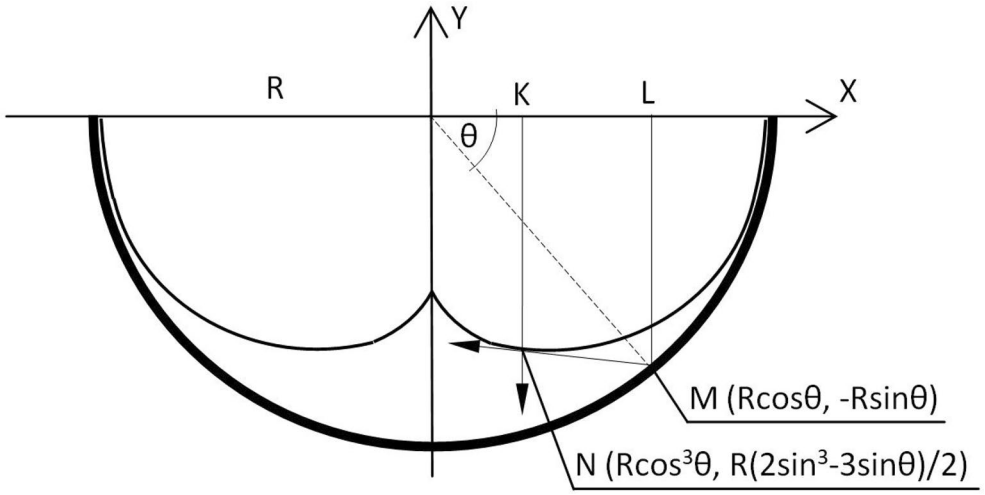

Fig. 6 Directions of the incident and reflected waves KN and LMN overlapping each other on the caustic [12]. The result is the sum of the sound pressures. R: radius of the reflector

According to the law of reflection, the reflected wave is tangent to the caustic. The distances SKN and SLMN travelled by the incident and reflected waves are

$$\begin{aligned} S_{KN} &= \frac{R}{2}|2\sin^3\theta - 3\sin\theta| \\ &= \frac{R}{2}\left(3\sin\theta - 2\sin^3\theta\right), \quad 0 \geq \theta \geq \Pi \end{aligned} \tag{15}$$

$$\begin{aligned} S_{LMN} &= R\sin\theta + \sqrt{\left(R\cos\theta - R\cos^3\theta\right)^2 + \left(-R\sin\theta - \left(\frac{R}{2}\left(2\sin^3\theta - 3\sin\theta\right)\right)\right)^2} \\ &= R\sin\theta + \sqrt{\left(\frac{R}{2}\sin\theta\sin 2\theta\right)^2 + \left(\frac{R}{2}\sin\theta\cos 2\theta\right)^2} \\ &= R\sin\theta + \frac{R}{2}\sin\theta\sqrt{(\sin 2\theta)^2 + (\cos 2\theta)^2} = \frac{3}{2}R\sin\theta, \quad 0 \geq \theta \geq \Pi \end{aligned} \tag{16}$$

In spite of the essentially different nature of acoustic and electromagnetic waves, the general principles of wave motion describe the energetic relationships of acoustic and electromagnetic waves using the same equations, differing only in the physical interpretation of the individual components. Substantial difference concerns the superposition of waves, which is scalar or vector in nature for acoustic or electromagnetic waves, respectively. In order to facilitate the comparison of the energetic equations for both types of field, they are presented side by side.

The sound intensity I_s and surface power density of the electromagnetic field I_e, both in [W/m^2], are proportional to the squared sound pressure p^2 [Pascal] and squared amplitude of the electric field E[V/m], respectively

$$I_s = p^2/(\rho c_s) \tag{17}$$

$$I_e = E^2/(\mu_o c_l) \tag{18}$$

where ρ: density of the medium, [kg/m^3], c_s: speed of sound (in the air at atmospheric pressure and a temperature of 15 °C, $c_s = 331$ m/s, $\rho c_s = 415$[kg/(m^{2}s)]), μ_o: vacuum permeability ($\mu_o = 4\Pi 10^{-7}$, [H/m]), c_l: speed of light ($c_l = 3{*}10^8$ [m/s]).

So the amplitudes $p_c(\theta)$ and $E_c(\theta)$ of the sound pressure and the electric field's, respectively, on the caustic are

$$p_c(\theta) = \sqrt{I_{c,s}(\theta)\rho c_s} = \sqrt{I_o \rho c_s}\sqrt{\frac{2(1-\alpha)\sin(\theta)}{3|\cos^3(\theta)|}} \tag{19}$$

$$E_c(\theta) = \sqrt{I_{c,e}(\theta)\mu_0 c_l} = \sqrt{I_e \mu_0 c_l}\sqrt{\frac{2R\sin(\theta)}{3|\cos^3(\theta)|}} \tag{20}$$

where $I_{c,s}(\theta)$: sound intensity on the caustic, [W/m^2], $I_{c,e}(\theta)$: surface power density of the electromagnetic field on the caustic, [W/m^2], I_o: intensity of the incident sound, [W/m^2], I_e: surface power density of the incident wave, electromagnetic field, [W/m^2]. α: sound absorption coefficient, R: reflection coefficient of the electric component of the electromagnetic wave.

$$\alpha = \frac{I_{abs}}{I_i} = \left(\frac{\overline{p}_{abs}}{\overline{p}_i}\right)^2 \tag{21}$$

$$R = \left(\frac{\overline{E}_{refl}}{\overline{E}_i}\right)^2 \tag{22}$$

I_{abs}, I_i: intensity of the absorbed and incident acoustic wave, $\overline{p}_i$,$\overline{p}_{abs}$:sound pressure amplitude of the incident and absorbed acoustic wave, averaged over a spherical angle of 2Π steradians. $\overline{E}_i$,$\overline{E}_{refl}$: amplitude of the incident and reflected electric field, averaged over a spherical angle of 2Π steradians. For the sake of brevity, the total reflection of the electromagnetic wave, i.e. R = 1, was adopted in the article.

At the point in time t, the sound pressure p(t) and the amplitude of the electric field $E(t)$ of the incident acoustics and electromagnetic wave, respectively, in the plane y = 0 of the reflector are

$$p(t) = \sqrt{I_o \rho c_s} \sin \varpi t \tag{23}$$

$$E(t) = \sqrt{I_e \mu_0 c_l} \sin \varpi t \tag{24}$$

where ω = 2Πf, f: frequency, [Hz].

Assuming lossless wave propagation, after travelling the distance S_{KN} by the acoustic wave, the incident sound pressure p_i(t) is

$$p_i(t) = \sqrt{I_o \rho c_s} \sin \varpi (t + \Delta t_1) \tag{25}$$

$$\Delta t_1 = S_{KN}/c_s \tag{26}$$

and after travelling the distance S_{LMN}, the sound pressure p_{refl}(t) of the reflected wave on the caustic according to Eq. (19) is

$$p_{refl}(t,\theta) = \sqrt{I_o \rho c_s} \sqrt{\frac{2(1-\alpha)\sin(\theta)}{3|\cos^3(\theta)|}} \sin \varpi (t + \Delta t_2) \tag{27}$$

$$\Delta t_2 = S_{LMN}/c_s \tag{28}$$

The sound pressure p_{res}(t,θ) resulting from the scalar summation of the sound waves is

$$\begin{aligned} p_{res}(t,\theta) &= p_i(t) + p_{refl}(t,\theta) \\ &= \sqrt{I_o \rho c_s}\left(\sin \varpi (t + \Delta t_1) + \sqrt{\frac{2(1-\alpha)\sin(\theta)}{3|\cos^3(\theta)|}} \sin \varpi (t + \Delta t_2)\right) \end{aligned} \tag{29}$$

The rest of this point concerns the phenomena occurring in the acoustic field.

The path difference of the direct and reflected front of acoustic waves makes p_{res}(t,θ) to fluctuate on the caustic over time. The fluctuations are described by Eq. (30), which is obtained by substituting Eqs. (15), (16) to (26), (28) and then to (29).

$$\begin{aligned} p_{res}(t,\theta) = \sqrt{I_o \rho c_s}\Bigg[&\sin \varpi \left(t + \frac{R}{2c_s}\left(3\sin\theta - 2\sin^3\theta\right)\right) \\ &+ \sqrt{\frac{2(1-\alpha)\sin(\theta)}{3|\cos^3(\theta)|}} \sin \varpi \left(t + \frac{3R}{2c_s}\sin\theta\right)\Bigg] \end{aligned} \tag{30}$$

The fluctuations are in the form of amplitude modulation, the maximum range of which results from Eq. (31).

$$\frac{d}{dt} p_{res}(t,\theta) = 0 \tag{31}$$

For a given θ, Eq. (30) describes the fluctuations at a given point of the caustic. Solving Eq. (31) i.e. finding the function t(θ), determines the amplitude of the fluctuations on the entire caustic. The solution of Eq. (31) is given in Eq. (32). For details see the Appendix, Eq. (49).

$$t = \frac{1}{\varpi} \operatorname{arctg}(q) - \Delta t_1 \tag{32}$$

where

$$q = \frac{\sqrt{\frac{3|\cos^3\theta|}{2(1-\alpha)\sin\theta}} + \cos\left(\varpi \frac{R\sin^3\theta}{c_s}\right)}{\sin\left(\varpi \frac{R\sin^3\theta}{c_s}\right)} \tag{33}$$

Substituting t into Eq. (30) yields the maximum range of amplitude modulation of sound pressure $p_{res,Max}(\theta)$ [Pa] over the whole caustic.

$$p_{res,Max}(\theta) = \sqrt{I_o \rho c_s}\left[\sin\left(\operatorname{arctg}(q)\right) + \sqrt{\frac{2(1-\alpha)\sin(\theta)}{3|\cos^3(\theta)|}} \sin\left(\operatorname{arctg}(q) + \varpi \frac{R\sin^3\theta}{c_s}\right)\right] \tag{34}$$

Case studies

The mechanism of caustic formation and the circumstances of the focal formation, graphically shown by LdV in Fig. 1a, are shown in this section on real objects. The presented examples concern the formation of caustics indoors and in outdoor acoustic installations with a demonstration function. How the development of the receiving technique related to the detection of radio waves extended the mirror aperture estimated by LdV is also shown.

Caustics in sound field

Figure 7 a, b presents the graph of Eqs. (30) and (34) for sound waves with a frequency of f = 1000 Hz and f = 2000 Hz, reflected by a hemispherical reflector with the diameter of D = 2 m. In both cases, the wavelength

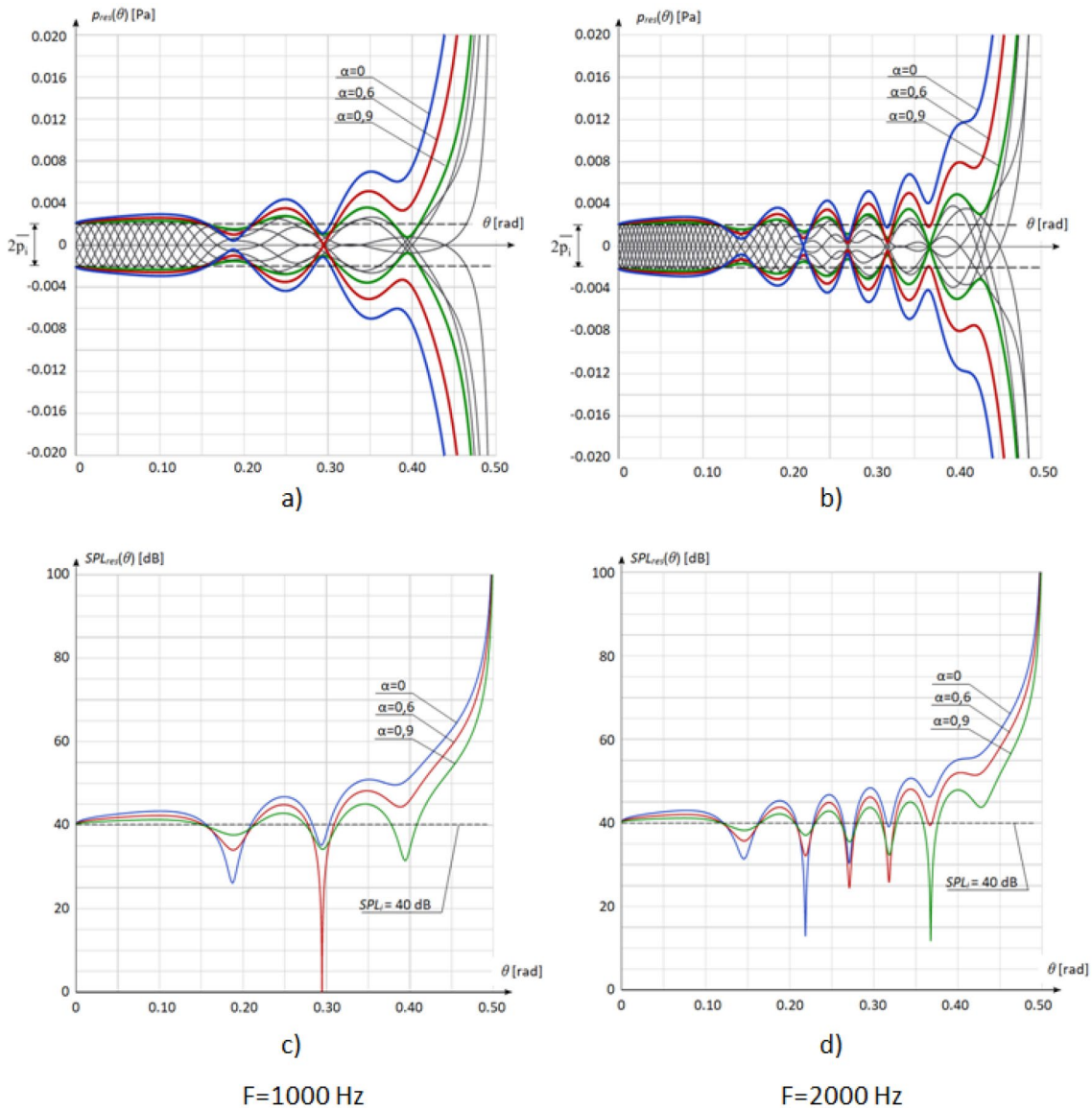

Fig. 7 **a**, **b** Resultant sound pressure of the plane waves with the frequencies f = 1000 Hz and f = 2000 Hz, respectively, incident on a hemispherical reflector with the radius R = 1 m and interfering with the wave that forms the caustic. $\overline{p_i}$: amplitude of the incident wave, α : sound absorption coefficient of the reflector. Thin black lines: sound pressure of the resultant wave $p_{res}(t,\theta)$ at the points in time t = 0, T/8, 7 T/8 where T = 1/f, at α = 0.9. Green, red and blue lines: amplitude of fluctuations $p_{res,Max}(\theta)$ at α = 0.9, α = 0.6 and α = 0, respectively. Due to symmetry, the range $0 \le \theta \le \Pi/2$ is shown. **c**, **d** Resultant sound pressure level $SPL_{res}(\theta)$ of the interfering waves described above. SPL_i: level of the incident wave

λ is much smaller than the diameter of the reflector D (λ/D = 0.17 and λ/D = 0.085, respectively). The directions of the waves shown in Fig. 6 therefore meet the principles of geometric optics, and the diffraction of the wave at the reflector's edge can be neglected.

Let us assume that the intensity of the incident wave I_o is 10^{-8} [W/m^2], which corresponds to sound pressure with an amplitude of 0.002 [Pa] and sound pressure level $SPL_i = 40$ dB re. 2×10^{-5} [Pa] (Eqs. 35, 36).

$$\overline{p_i} = \sqrt{I_o \rho c_s} = \sqrt{10^{-8} * 415} \cong 0.002 \quad [\text{Pa}] \tag{35}$$

$$SPL_i = 20 \log \left(0.002/(2 * 10^{-5}) \right) = 40 \ [\text{dB}] \tag{36}$$

The sound pressure p_{res} (Eq. 30) and the corresponding pressure level SPL_{res} (Eq. 37) fluctuate around these values. The amplitude of the fluctuations increases with the increasing effect of wave concentration on the caustic (Fig. 7 a, b).

$$SPL_{res}(\theta) = 20 \log \left(p_{res,\max}(\theta)/(2 * 10^{-5}) \right) \tag{37}$$

At the cusp of the caustic, the concentrated energy of the reflected waves significantly exceeds the energy of the incident wave, which reduces the fluctuation effect (Fig. 7 c, d).

The result of interference outside the focus is the arrangement of nodes and antinodes formed by the superimposition of incident and reflected waves on the caustic. In real conditions, its regularity shown in Fig. 7 is disturbed by the broadband nature of the sound and by the reverberant field of the room. This is combined with the diffraction of the incident low frequency wave at the edge of the canopy. As a result, the presence of caustics in the room is usually difficult to detect by hearing, and the audible effect of sound focussed by acoustic mirrors is reduced to a compact area of increased sound pressure.

Figure 7 shows how much sound amplification can be expected at the cusp of the caustic. When the level of incident sound on the mirror is about 40 dB, which corresponds to e.g. a quiet conversation (Fig. 7 c, d), the sound level felt in the focus is so high that this phenomenon can be used for acoustic demonstrations or for eavesdropping of conversations practiced in historical times. Figure 7 shows that in the focus, the surface sound power density may increase by approx. 45 dB or more, which is accounted for by a small part of the canopy. It is a computational illustration of LdV's concept, as shown in Fig. 2. The opening angle of the canopy in the original LdV drawing, for obvious reasons not supported by calculations, is approx. 10° .

The field installations found in educational parks are a contemporary implementation of LdV's observation (Fig. 8a). The whisper caves shown in Fig. 8b, apart from demonstrating the echo effect [10], also serve as an element of historical park architecture and a place of shelter from rain. Therefore, their shape is wider than required by the demonstrated phenomenon of reflection.

There are numerous architectural objects in which caustics are formed in the form shown in LdV's drawings. We are talking here primarily about historical interiors with a sacred and ceremonial function, containing

a) b)

Fig. 8 Outdoor installations erected to demonstrate acoustic curiosities. **a** Contemporary outdoor installation made by 3D printing [15–17], photo courtesy of M. Kladeftira. **b** Eighteenth-century Whispering Grottoes in Oliwa Park, Gdańsk, Poland [10, 14], photo courtesy of T. Strug

Fig. 9 Historical rooms with large dome-shaped areas. **a** Hagia Sophia in Istanbul, Turkey, photo courtesy of Keep & Share, [18]. **b** Dome of the Rock in Jerusalem, Israel, ©CC by 2.0 [30]

large areas in the form of a dome (Fig. 9). Caustics in the described form were also created in Nineteenth-century theaters and concert halls with concave vaults, which were the then canon of the neo-renaissance style (Fig. 10) [12].

Caustics in electromagnetic fields

The Arecibo radio telescope in Puerto Rico (Fig. 11) was put into operation in 1963 and initially the reflector aperture was small. It was significantly upgraded in 1997 by the use of the Gregorian subreflector system, which concentrates the energy of the caustics sections adjacent to the cusp into the single focal point (Fig. 12). The subreflector system consists of two shaped surfaces called secondary and tertiary reflectors hidden inside on the geodetic dome. The first is the parabolic reflector and the second constitutes the pair of elliptic reflectors (Fig. 13) [20].

The upgraded aperture of the $A_{Arecibo}$ radio telescope is approx. 30,000 m^2, which is approx. 7% of the hemisphere surface with a radius of $R_{Arecibo} = 265$ m (Eq. (38)) [21].

$$\frac{A_{Arecibo}}{2\Pi R_{Arecibo}^2} = \frac{30000}{2\Pi 265^2} = 0.068 = 6.8\% \tag{38}$$

Compared to the reflector analysed by LdV with an aperture of approx. 0.4% of the hemisphere area (see Fig. 3, Eqs. 1 and 2), the relative aperture of the Arecibo radio telescope reflector is 17 times greater (0.068/0.004 = 17), i.e. by 1 order of magnitude. This is due to the fact that, according to LdV, the energy concentrated by the reflector is contained in its focus, while the Arecibo radio telescope enlarges it by the energy of a significant part of the caustic.

Prior to upgrading the Arecibo telescope, the receiver recorded the reflected wave concentrated in the focus and the wave coming from space. After the telescope was upgraded with the Gregorian subreflectors, receiver hidden inside on the geodetic dome is shielded by the secondary reflector as well as by the geodetic dome itself (Fig. 13) and does not record space signal. This change, however, is negligible, as the level of the signal concentrated in the focus exceeds the level of the space signal by several dozen dB (see Fig. 5).

On December 1, 2020—a tragic day for the scientific community—the Arecibo radio telescope was destroyed due to the cables breaking and the 900-ton main platform falling onto the radio telescope's canopy.

Parabolic reflector

In 2016, 53 years after the radio telescope in Arecibo was launched, the FAST radio telescope (Five-hundred-meter Aperture Spherical radio Telescope) was put into operation in Dawodang (China). Its antenna with a diameter of 520 m is a section of a sphere with a radius of $R_{FAST} = 300$ m (Fig. 14). A receiver weighing 3 tons, which moves over the dish by a system of cables, enables the observation of radio-sources contained in a cone with an opening angle of aperture of 80 degrees. The FAST radio telescope is a receiving device, while the Arecibo radio telescope was a transmitting and receiving device [25].

The canopy of the FAST radio telescope consists of 4500 movable elements, the position of which can be corrected in such a way that a selected part of the spherical reflector is transformed into a paraboloid segment (Fig. 15), including a circle with a diameter of 300 m.

a)

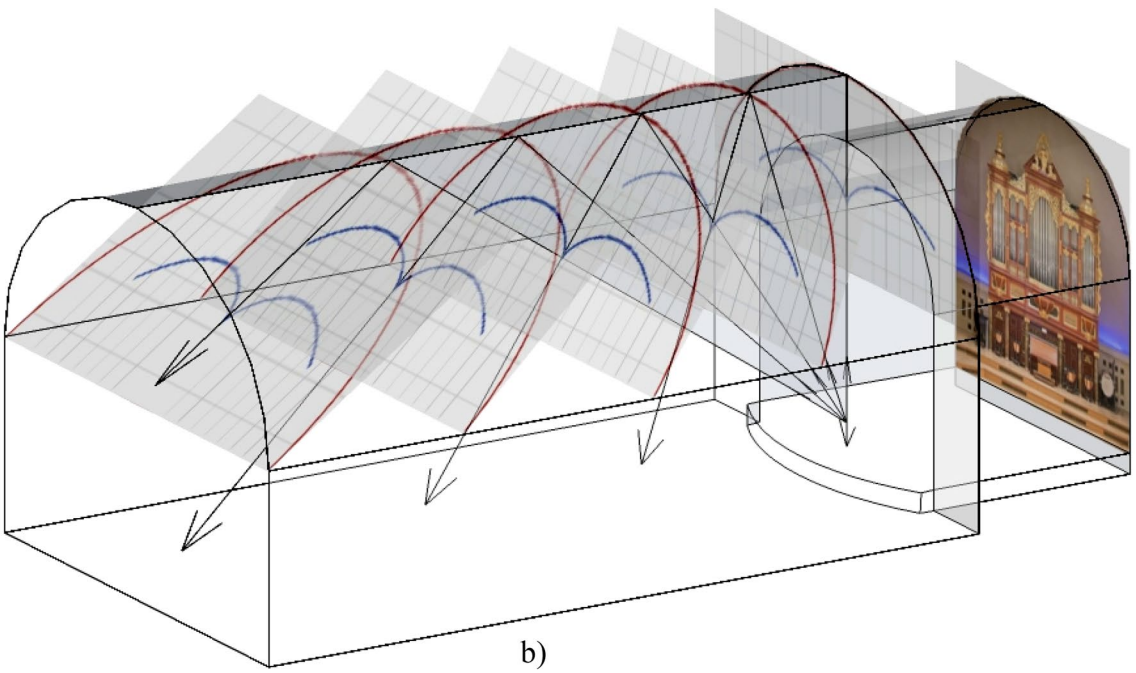

b)

Fig. 10 **a** Assembly Hall of Poznań University. This neo-renaissance building was erected according to the design of Edward Fürstenau in 1905–1910, photo courtesy of Poznań Film Commission [19]. **b** Cross-sections of a 3D caustic as predicted by LdV [12]

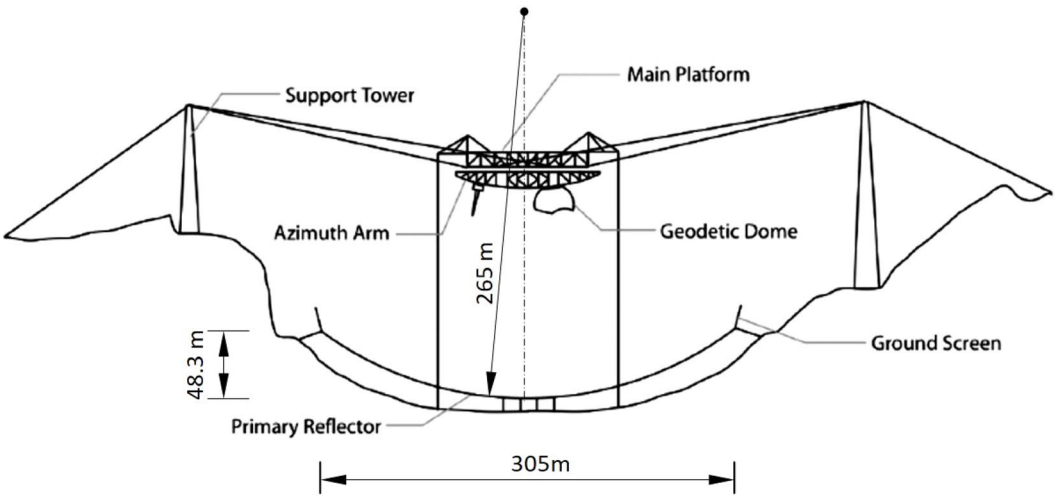

Fig. 11 Spherical radio telescope in Arecibo, Puerto Rico, photo taken before 01.12.2020 [22] Photo by the Public Domain of the National Space Foundation Multimedia Gallery. Below: diagram of the Arecibo telescope [20]

The corrected part of the reflector thus creates an aperture with a diameter of $A_{FAST} = 300$ m and a depth of $D_{FAST} = 40.2$ m [26], which gives an area of approx. 38,000 m^2, i.e. approx. 6.7% of the hemisphere area (Eqs. 39, 40). This shows a different direction of upgrade of LdV's concept over Arecibo. It involves manipulating the curvature of the reflector, while in Arecibo, the useful range of the caustic was manipulated.

$$2\Pi \times \tfrac{1}{2} A_{FAST} \times D_{FAST} = 2\Pi \times 150 \times 40.2 \approx 38000 m^2 \quad (39)$$

$$\frac{38000}{2\Pi R_{FAST}^2} = \frac{38000}{2\Pi 300^2} = 0.067 = 6.7\% \quad (40)$$

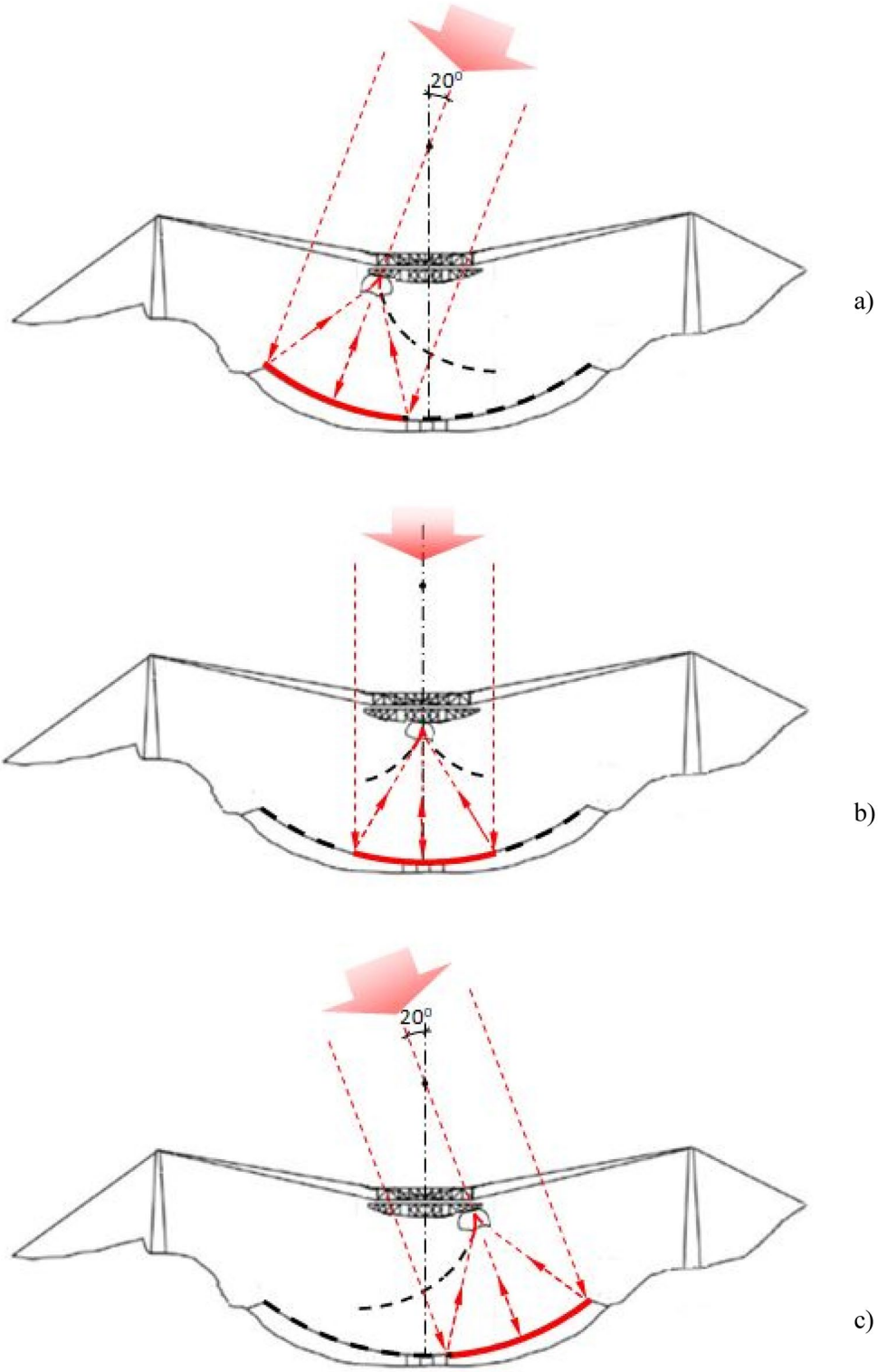

Fig. 12 Bowl of the Arecibo reflector and the caustic it forms. The active part of the reflector and caustics is shown (red). **a**, **b**, **c** Directions of wave arrival − 20°, 0°, + 20° relative to the zenith. Illustrative sketch based on [20]

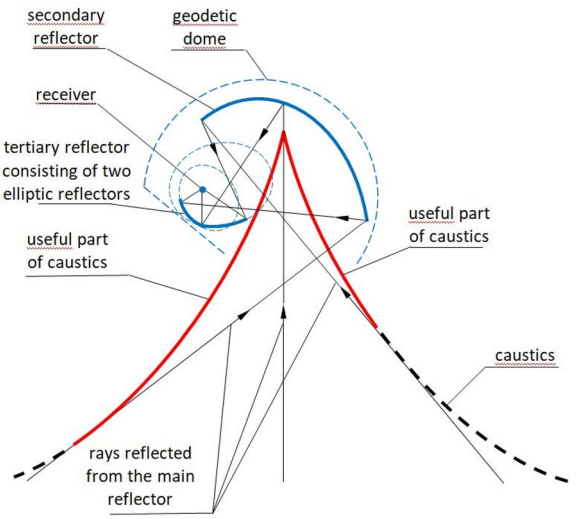

Fig. 13 Ray tracing of the secondary and tertiary reflectors of the Arecibo Gregorian Optics [23]. In addition to the energy of the focus, the Gregorian subreflector system also uses the energy concentrated on the part of caustic marked in red. The pair of ellipses defining the shape of the tertiary reflector is shown

The caustics present in the LdV sketches, also known a spherical aberration, are treated as a limitation in the use of a spherical mirror. In the case of a parabolic mirror, such a limitation is a coma aberration. It occurs when the observed object is located off the mirror axis and consists in blurring the focus into a loop caustic called a coma (Fig. 16). In a spherical mirror, aberration is an irremovable element of its functioning, while in a parabolic mirror, it disappears completely with the axial incidence of the rays. In the FAST radio telescope, the coma aberration is limited by positioning the receiver with a few-millimetre accuracy, with a deviation from the paraboloid axis not exceeding 8 arc seconds [27].

Concluding remarks

In the achievements of many leading fields of science, you can find ideas from hundreds of years ago, often coming from areas unrelated to the field. The article shows the presence of the concept of reflecting light by a spherical mirror, formulated by Leonardo daVinci about 500 years ago, in the development of seemingly distant fields of science and technology, such as acoustics and radio astronomy.

Leonardo conducted his theoretical research using a spherical mirror. He showed that less than 0.5% of the hemisphere area is enough to concentrate energy coming from an infinitely distant source, e.g. from the Sun. With the application of this mirror, the rest of the canopy is useless. This idea, obvious from the point of view of modern knowledge, but formulated 500 years ago, is present today in many areas of technology and science—the aperture of modern spherical mirrors is only a small part of the hemisphere. Their functioning in the field of architectural acoustics, in optical instruments, as antennas in radio telescopes, etc., is fully in line with the LdV predictions.

During the research on the phenomenon of light concentration, LdV showed a method of graphically determining the surface accompanying the focus, on which the reflected rays are concentrated. This surface is known today as a caustic and is present in many fields of technology and science. LdV, however, did not develop the idea of caustics, being apparently unaware of the importance of his discovery. In modern technical knowledge, you can encounter both of the above-mentioned elements of the functioning of mirrors discovered by LdV, i.e. foci and caustics. In the example shown in the article, when the caustic energy is added to the focal energy, the aperture increases from the approx. 0.5% predicted by LdV to approx. 5–7%. After local adjustment of the spherical mirror surface to the curvature of the parabola, the aperture increases to a similar extent. The aperture of the mirror determined by LdV has therefore undergone a significant upgrade as a result of the development of receiving techniques. The technical implementation of the described improvements are the 300 m radio telescope in Arecibo (Puerto Rico) and the 500 m FAST radio telescope in Dawodang (China). Internet reports inform about the concept of building a 1000 m radio telescope, located on the dark side of the Moon away from the Earth's electromagnetic smog, but due to the early stage of this idea, it is not discussed in the article [29].

The caustics found in LdV's drawings are also formed in acoustic field indoors. However, wave phenomena occurring in a room, reverberation and noise floor make it difficult to audibly identify the caustics. As a result, the effect of sound focusing by large curved surfaces in rooms, e.g. arched vaults and concave walls, is reduced to a point focus at the caustic cusp, and the rest of the caustic becomes inaudible. For this reason, the concept of caustics is almost unknown in the field of architectural acoustics.

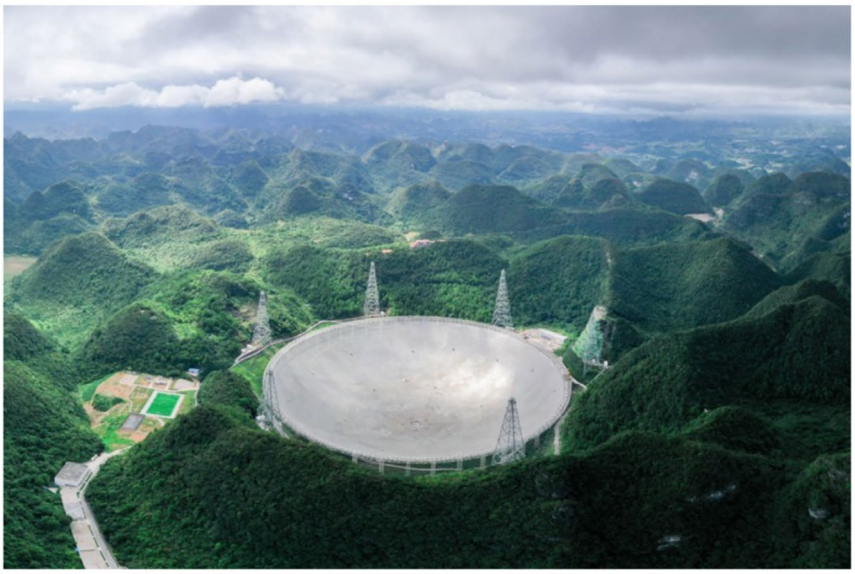

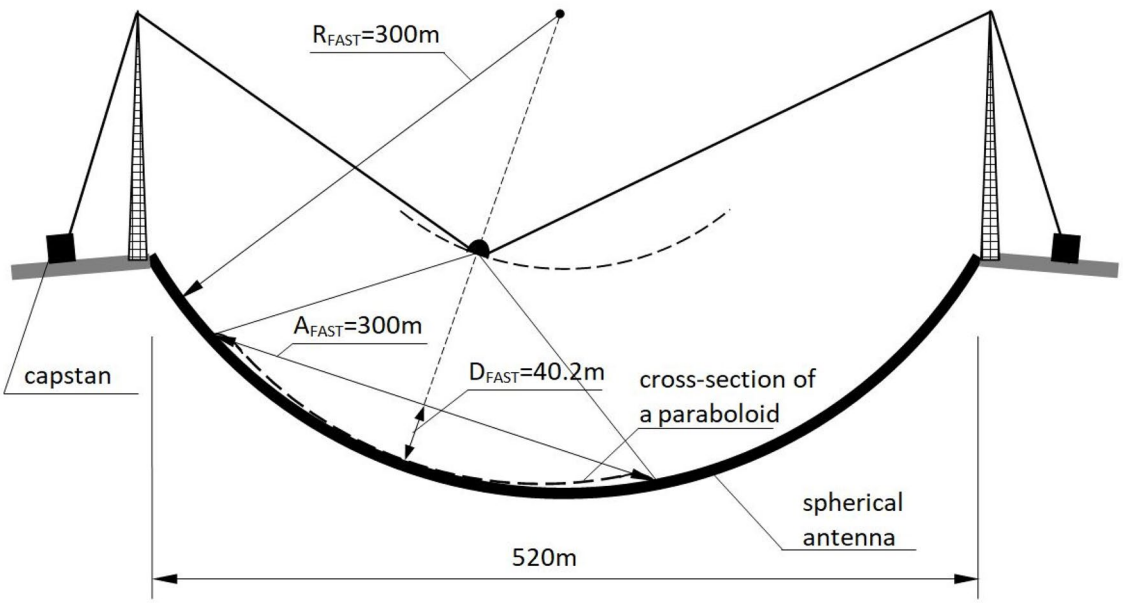

Fig. 14 Five-hundred-metre antenna of the FAST radio telescope [24]. Photo by permission from Springer Nature, license number 5315900703664. Below: a diagram of the FAST telescope [27]

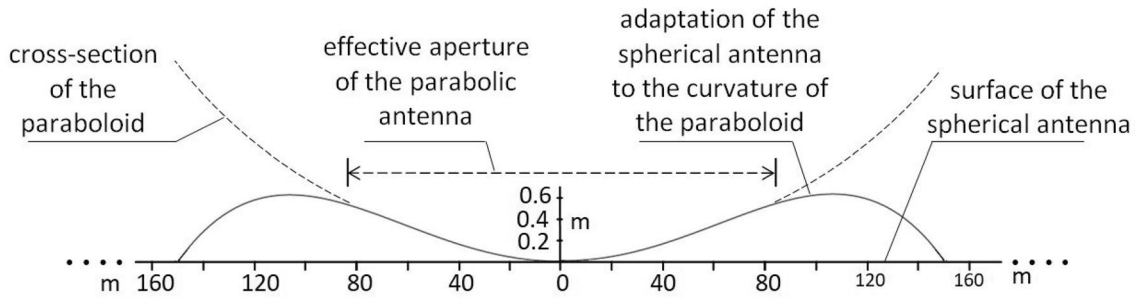

Fig. 15 One of the tested solutions, showing how to adapt a section of the spherical mirror of the FAST radio telescope to the curvature of the paraboloid [26]

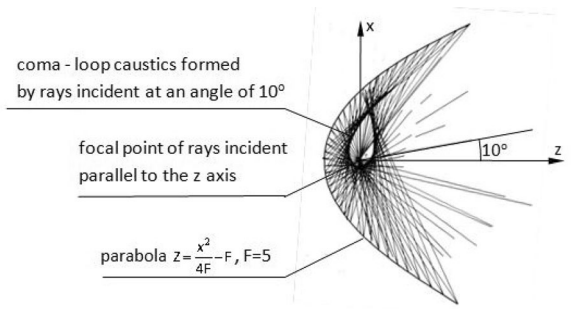

Fig. 16 Cross-section of a parabolic mirror with its typical distortion in the form of comatic aberration. When the source is located off the mirror axis, the focal point takes the form of a loop caustic, known as a coma [28]

Appendix

$$\frac{\mathrm{d}}{\mathrm{d}t}p_{c,res}(\mathrm{t},\theta)=\frac{\mathrm{d}}{\mathrm{d}t}\left[\sqrt{\mathrm{I_o}\rho\mathrm{c_s}}\left(\sin\left(\varpi(\mathrm{t}+\Delta\mathrm{t_1})\right)+\sqrt{\frac{2(1-\alpha)\sin(\theta)}{3|\cos^3(\theta)|}}\sin\left(\varpi(\mathrm{t}+\Delta\mathrm{t_2})\right)\right)\right]= \tag{41}$$

$$\sqrt{\mathrm{I_o}\rho c_s}\varpi\left(\cos\left(\varpi(\mathrm{t}+\Delta\mathrm{t_1})\right)+\sqrt{\frac{2(1-\alpha)\sin(\theta)}{3|\cos^3(\theta)|}}\cos\left(\varpi(\mathrm{t}+\Delta\mathrm{t_2})\right)\right)=0$$

Substituting,

$$\tau=\mathrm{t}+\Delta\mathrm{t_1} \tag{42}$$

and

$$\mathrm{b}=\sqrt{\frac{2(1-\alpha)\sin(\theta)}{3|\cos^3(\theta)|}} \tag{43}$$

yields,

$$\cos\varpi(\tau)=-\,\mathrm{b}\cos\varpi(\tau-(\Delta\mathrm{t_1}-\Delta\mathrm{t_2})) \tag{44}$$

and after expansion,

$$\cos\varpi(\tau)=-\,\mathrm{b}\left[\cos(\varpi\tau)\cos\left(\varpi(\Delta\mathrm{t_1}-\Delta\mathrm{t_2})\right)+\sin(\varpi\tau)\sin\left(\varpi(\Delta\mathrm{t_1}-\Delta\mathrm{t_2})\right)\right] \tag{45}$$

regrouping yields,

$$\frac{\sin(\varpi\tau)}{\cos(\varpi\tau)}=\frac{\frac{1}{\mathrm{b}}+\cos\left(\varpi(\Delta\mathrm{t_1}-\Delta\mathrm{t_2})\right)}{-\sin\left(\varpi(\Delta\mathrm{t_1}-\Delta\mathrm{t_2})\right)} \tag{46}$$

and then,

$$\varpi(\mathrm{t}+\Delta\mathrm{t_1})=\mathrm{arctg}\left(\frac{\frac{1}{\mathrm{b}}+\cos\left(\varpi(\Delta\mathrm{t_1}-\Delta\mathrm{t_2})\right)}{-\sin\left(\varpi(\Delta\mathrm{t_1}-\Delta\mathrm{t_2})\right)}\right) \tag{47}$$

since,

$$\Delta\mathrm{t_1}-\Delta\mathrm{t_2}=\frac{\frac{\mathrm{R}}{2}\left(3\sin\theta-2\sin^3\theta\right)}{\mathrm{c_s}}-\frac{\frac{\mathrm{R}}{2}3\sin\theta}{\mathrm{c_s}}=-\frac{\mathrm{R}\sin^3\theta}{\mathrm{c_s}} \tag{48}$$

$$\mathrm{t}=\frac{1}{\varpi}\mathrm{arctg}\left(\frac{\sqrt{\frac{3|\cos^3\theta|}{2(1-\alpha)\sin\theta}}+\cos\left(\varpi\frac{\mathrm{R}\sin^3\theta}{\mathrm{c_s}}\right)}{\sin\left(\varpi\frac{\mathrm{R}\sin^3\theta}{\mathrm{c_s}}\right)}\right)-\Delta\mathrm{t_1} \tag{49}$$

Abbreviations
LdV: Leonardo da Vinci; FAST: Five-hundred-meter aperture spherical radio telescope.

Acknowledgements
Not applicable

Author contributions
Not applicable.

Funding
Not applicable.

Availability of data and materials
Not applicable.

Declarations

Competing interests
The author declare that he has no competing interests.

Received: 26 December 2021 Accepted: 7 May 2022
Published online: 05 July 2022

References

1. http://www.unmuseum.org/burning_mirror.htm. Accessed 29 Sept 2021.
2. https://en.wikipedia.org/wiki/Ptolemy. Accessed 29 Sept 2021.
3. Raynaud Dominique. The aerial perspective of Leonardo da Vinci and his origins in the optics of Ibn al-haytham (de aspectibus, III, 7). Arab Sci Philos. 2009;19(2):225–46.
4. Ivanov VP, Ivanova GK. Caustic structure of the underwater sound channel. Open Journal of Acoustics, 4, 26–37. 2014. http://file.scirp.org/pdf/OJA_2014032115460011.pdf. Accessed 29 Sept 2021.
5. Khatkevich AG, Khatkevich LA. Propagation of laser beams and caustics in crystals. Journal of applied spectroscopy, 74, No. 4. 2007. https://link.springer.com/article/10.1007/s10812-007-0086-8. Accessed 29 Sept 2021.
6. Skowron J. Analiza niestandardowych zjawisk mikrosoczewkowania grawitacyjnego gwiazd Galaktyki. Rozprawa doktorska (Analysis of non-standard phenomena of gravitational microlensing of Galactic stars. PhD dissertation, in Polish). Uniwersytet Warszawski. 2009. http://www.astro.uw.edu.pl/~jskowron/PhD/thesis/phd.pdf. Accessed 13 Nov 2021.
7. http://www.bl.uk/turning-the-pages/?id=cb4c06b9-02f4-49af-80ce540836464a46&type=book. The Leonardo notebook, pp. 8–15. Accessed 29 Sept 2021.
8. http://www.bl.uk/turning-the-pages/?id=cb4c06b9-02f4-49af-80ce540836464a46&type=book,%20p.%208%E2%80%9314, Leonardo da Vinci's Codex Arundel, pp. 224–226, 414. Accessed 29 Sept 2021.
9. Leonardo da Vinci's studies of reflections from concave mirrors ff.86v-87. pages11and12.html. http://www.bl.uk/onlinegallery/ttp/leonardo/accessible/. Accessed 08 June 2022.
10. Kulowski A. The caustic in the acoustics of historic interiors. Appl Acoust. 2018;133:82–90. https://doi.org/10.1016/j.apacoust.2017.12.008.
11. Leonardo da Vinci's studies of reflections from concave mirrors ff.87v-88. pages13and14.html. https://www.bl.uk/onlinegallery/ttp/leonardo/accessible/. Accessed 08 June 2022.
12. Kulowski A. Analysis of a caustic formed by a spherical reflector: impact of a caustic on architectural acoustics. Appl Acoust. 2020. https://doi.org/10.1016/j.apacoust.2020.107333.
13. Burkhard DG, Shealy DL. Formula for the density of tangent rays over a caustic surface. Appl Opt. 1982;21(18):3299–306.
14. https://staraoliwa.pl/. Accessed 31 May 2022.
15. https://dbt.arch.ethz.ch/project/acoustic-mirrors/. Accessed 16 Aug 2020.
16. Kladeftira M. et al. Design strategies for a 3D printed acoustic Mirror Proc of the 24th CAADRIA conference-Vol 1. Wellington: Victoria University of Wellington; 2019. p. 123–132.
17. Kladeftira M et al. Printing whisper dishes. Large-scale binder jetting for outdoor installations. Proc of the ACADIA 2018 recalibration: on imprecision and infidelity, Proc of the 38th annual conference of the association for computer aided design in architecture. Mexico City; 2018. p. 328–35.
18. https://www.keepandshare.com/photo/382500/hagia-sophia?ifr=y. Accessed 31 May 2022.
19. http://poznanfilmcommission.pl/lokacja/aula-uam. Accessed 21 Sept 2019.
20. https://www.researchgate.net/figure/A-diagram-of-the-Arecibo-telescope_fig1_2209614. Accessed 29 Sept 2021.
21. Magnani L. The arecibo 5GHz mini-gregorian feed system; spectral line performance. Publ Astron Soc Pac. 1993;105(690):894–901.
22. https://www.space.com/38217-arecibo-observatory-puerto-rico-telescope-photos.html. Accessed 29 Sept 2021.
23. Cortés-Medellín G. AOPAF: arecibo observatory phased array feed. Internet publication by national astronomy and ionosphere center cornell university. 2010. https://www.naic.edu/~phil/hardware/byuPhasedAr/logs/Cortes%20AOPAF_short%20report%20Sept%202010-1.pdf. Accessed 29 Sept 2021.
24. https://www.nature.com/articles/d41586-019-02790-3. Accessed 29 Sept 2021.
25. Mathews JD. A short history of geophysical radar at Arecibo Observatory. Hist Geo- Sp Sci. 2013;4(1):19–33. https://doi.org/10.5194/hgss-4-19-2013.
26. Nan R, Li D et al. The five-hundred-meter aperture spherical radio telescope (FAST) project, international journal of modern physics D, ©World Scientific Publishing Company. https://arxiv.org/ftp/arxiv/papers/1105/1105.3794.pdf. Accessed 29 Sept 2021.
27. Williams II RL. "Five-Hundred Meter Aperture Spherical Radio Telescope (FAST) Cable-Suspended Robot Model and Comparison with the Arecibo Observatory". www.ohio.edu/people/williar4/html/pdf/FAST.pdf. Accessed 29 Sept 2021.
28. Schmidt RF. Analytical caustic surfaces. NASA technical memorandum 87805. NASA technical reports server. 1987. https://ntrs.nasa.gov/archive/nasa/casi.ntrs.nasa.gov/19880001678.pdf. Accessed 29 Sept 2021.
29. https://www.nasa.gov/directorates/spacetech/niac/2020_Phase_I_Phase_II/lunar_crater_radio_telescope/. Accessed 26 Oct 2021.
30. Wikimedia Commons. https://commons.wikimedia.org/wiki/File:Al_Aqsa_(6888221391).jpg (cropped). Accessed 31 May 2022.

Publisher's Note